

Article

## Exploration of the Dynamical Evolution and the Associated Energetics of Water Nanoclusters Formed in a Hydrophobic Solvent

Rajib Kumar Mitra, Pramod Kumar Verma, and Samir Kumar Pal

*J. Phys. Chem. B*, **2009**, 113 (14), 4744-4750 • DOI: 10.1021/jp8085705 • Publication Date (Web): 16 March 2009

Downloaded from <http://pubs.acs.org> on April 7, 2009

### More About This Article

Additional resources and features associated with this article are available within the HTML version:

- Supporting Information
- Access to high resolution figures
- Links to articles and content related to this article
- Copyright permission to reproduce figures and/or text from this article

[View the Full Text HTML](#)

# Exploration of the Dynamical Evolution and the Associated Energetics of Water Nanoclusters Formed in a Hydrophobic Solvent

Rajib Kumar Mitra, Pramod Kumar Verma, and Samir Kumar Pal\*

Unit for Nano Science & Technology, Department of Chemical, Biological & Macromolecular Sciences, S. N. Bose National Center for Basic Sciences, Block JD, Sector III, Salt Lake, Kolkata 700098, India

Received: September 27, 2008; Revised Manuscript Received: January 22, 2009

Exploration of the intermolecular binding energy in nanometer-sized small water clusters in hydrophobic solvents and its evolution with the increase in the cluster size until bulk-type geometry is reached constitute a fascinating area of research in contemporary chemical/biological physics. In this contribution we have used femtosecond/picosecond-resolved solvation dynamics and fluorescence anisotropy techniques to explore the dynamical evolution of water clusters in dioxane continuum as a function of water concentration. We have also used temperature dependent picosecond-resolved solvation dynamics in order to explore the magnitude of the intermolecular bonding energy in the water clusters in bulk dioxane.

## Introduction

Water has anomalous properties that emanate from its hydrogen-bond-induced structure (clusters). Most of the unique properties of water are related to the network of strong three-dimensional hydrogen bonds that interconnect the water molecules.<sup>1,2</sup> According to Stillinger,<sup>3</sup> water has a preferential three-dimensional tetrahedral structure containing a few free or single-bonded water molecules. Liquid water represents a disordered ensemble of highly polar molecules linked through a fluctuating network of intermolecular hydrogen bonds on femtosecond to picosecond time scales as evidenced from the pioneering works by Elsaesser et al.,<sup>4–7</sup> Wiersma et al.,<sup>8,9</sup> Voehringer et al.,<sup>10</sup> Fayer et al.,<sup>11</sup> Tokmakoff et al.<sup>12</sup> using ultrafast vibrational spectroscopy and MD simulation studies, and Bekker et al.<sup>13,14</sup> using time-resolved pump–probe laser spectroscopy measurements. The slowest component of the fluctuations is associated with the global structural rearrangement of the hydrogen bond network.<sup>15</sup> It is known that water molecules tend to form clusters in many organic solvents, and the existence of clusters even in the presence of a trace amount of water has recently been proved.<sup>16,17</sup> Depending upon the external environment, the size and geometry of the small clusters may vary from dimer to octamer with varying geometry.<sup>18</sup> The exact nature of the clusters is still a subject of clarification. There is strong doubt about the structure of the clusters, whether it is micelle-like<sup>19–22</sup> or not.<sup>17</sup> How this change in the cluster geometry affects water dynamics and water-mediated reaction are challenging questions to be addressed.

Water in hydrophobic environment forming very small clusters of 2–10 water molecules<sup>23</sup> can give rise to properties different from the bulk properties<sup>24–26</sup> with entropy and weak Van der Waals interaction playing a crucial role.<sup>27–29</sup> Such a system provides a rare opportunity for studying solution properties, including the dynamic translational and rotational motions of water molecules without the effect of hydrogen bonding to the surrounding water molecules.<sup>30</sup> Such a situation mimics the dynamical behavior of the isolated water molecules in biological systems like lipid bilayer, protein interior, etc.<sup>31</sup> The affinity of polar water molecules toward a hydrophobic

surface is striking, and the dynamics of such isolated water molecules (or small clusters) are interesting topics of investigation. Such clusters reorganize themselves in a cooperative way on ultrafast time scales, typically on the order of picoseconds. Although such dynamics in neat polar solvents has been studied both experimentally<sup>4,32</sup> and using molecular dynamic simulation,<sup>33,34</sup> those involving more than one solvent are sparse. Earlier studies involving binary mixtures show that the solvation time scale varies markedly with the composition of the mixture.<sup>35,36</sup> Levinger et al. showed that in a mixture of dipolar and quadrupolar solvents, the solvation dynamics is strongly affected by the differences in interaction energies and the relaxation rate of individual components.<sup>37</sup> A similar conclusion was drawn by Ladanyi et al.<sup>38</sup> using MD simulation for the same system. Only a handful of studies involving water clusters in nonpolar solvents are reported in the present literature,<sup>16,17</sup> especially at rather low free water concentrations found in moderately polar (e.g., biological) environments. As the water cluster grows in size, the initial unfavorable energy of formation of clusters decreases and hydrogen bond formation initiates between water molecules.<sup>23</sup> Water clusters in 1,4-dioxane (DX) have been reported to exhibit slow solvation dynamics of the order of a few hundreds of picoseconds.<sup>39–41</sup> This slow solvation has been explained as due to the translational motion of water, and the rupture of a hydrogen bond between DX and water has been identified to be the rate-determining step.

DX has a unique property to solubilize water in all proportions in spite of its negligible polarity (static relative permittivity of 2.2095), and it also offers a substantial number of noninteracting hydrophobic sites ( $-C_2H_4$  segments) to water. This makes the mixture an interesting environment to study the dynamics of water in hydrophobic confinement. Also DX can form hydrogen bonds with water but cannot self-associate to form clusters. The structural evolution of water clusters in DX continuum as a function of water concentration has earlier been studied using the laser light scattering (LLS) technique<sup>20</sup> and IR spectroscopy.<sup>42</sup> LLS measurement reveals the presence of nanometer-sized water clusters in DX continuum at low water concentrations as evidenced from the diffusion constant measurements. The IR study reveals that with increasing water content, the IR spectra of the cluster tend toward that of the bulk water. At

\* Corresponding author. E-mail: skpal@bose.res.in.

low water concentration, a weak component of free OH bond at  $3685\text{ cm}^{-1}$  was obtained confirming the presence of weakly hydrogen-bonded (isolated) water molecules. Beyond a threshold water concentration corresponding to  $X_W = 0.2$  (where  $X_W$  is the mole fraction of water in the mixture), the system provided the signature of pure liquid water. The observed dramatic increase in the integral water extinction coefficient in a narrow range of water concentration ( $X_W = 0.2$ ) indicates the formation of new hydrogen bonds between water molecules as the cluster grows in size as hydrogen bonding leads to a drastically increased integrated intensity of the OH oscillator stretching vibration band.<sup>43</sup> Thus a change in the water properties in clusters beyond this threshold  $X_W$  is expected. How the dynamics of water evolves with the change in hydrogen bond formation around this threshold concentration is a question of interest. The earlier reports<sup>39–41</sup> on the slow picosecond-resolved solvation of water–DX mixture are concerned with the concentrated regions ( $X_W \geq 0.22$ ) of the mixture. However, what happens when the hydrogen bonds are not well established in small clusters has not yet been studied. How this change in cluster configuration and a corresponding alteration of hydrogen bond formation are manifested in the dynamics of water molecules is the main focus of the present work.

Here we have studied the dynamics of water molecules in water–DX mixture on femtosecond and picosecond time scales at different water concentrations ( $X_W = 0.005, 0.025, 0.2, 0.54,$  and  $0.826$ ) using a well-known solvation probe coumarin 500 (C500). Note that we have chosen concentrations both below ( $X_W = 0.005, 0.025$ ) and above ( $X_W = 0.54, 0.826$ ) the threshold concentration ( $X_W = 0.2$ ) as mentioned above to understand the nature of solvation as a function of the modification of cluster size as well as the nature of hydrogen bonding. The choice of the probe lies in the fact that when excited with a wavelength of  $409\text{ nm}$ , the probes residing in the polar region get selectively excited.<sup>44,45</sup> Insignificant interference of the internal photophysics of the probe in the exploration of solvation dynamics has already been discussed in our earlier works.<sup>45–48</sup> While femtosecond-resolved fluorescence upconversion technique explores the ultrafast rotation/internal motions, the picosecond-resolved time-correlated single photon counting (TCSPC) method measures the diffusive translational motion of the water molecules. Polarization-gated fluorescence anisotropy of the probe molecules (C500) in the femtosecond and picosecond time regime has also been measured to explore the local microviscosity of the water clusters. To understand the energetics of the hydrogen bond network in the clusters, we have also studied solvation dynamics of water at different temperatures at  $X_W = 0.2$ .

## Materials and Methods

1,4-Dioxane (DX) was purchased from Merck and was of the highest purity available and used without further purification. The probe coumarin 500 (C500) was a product of Exciton. Triply distilled water with conductivity less than  $2\ \mu\text{S cm}^{-1}$  was used.

Steady-state absorption and emission spectra were measured with a Shimadzu UV-2450 spectrophotometer and Jobin Yvon Fluoromax-3 fluorimeter, respectively, with temperature controller attachment from Julabo (model: F32). Femtosecond-resolved fluorescence spectroscopy was measured using a femtosecond upconversion setup (FOG 100, CDP) in which the sample was excited at  $410\text{ nm}$ , using the second harmonic of a mode-locked Ti-sapphire laser with an  $80\text{ MHz}$  repetition rate (Tsunami, Spectra Physics), pumped by  $10\text{ W}$  Millennia (Spectra Physics). The fundamental beam was frequency doubled in a nonlinear

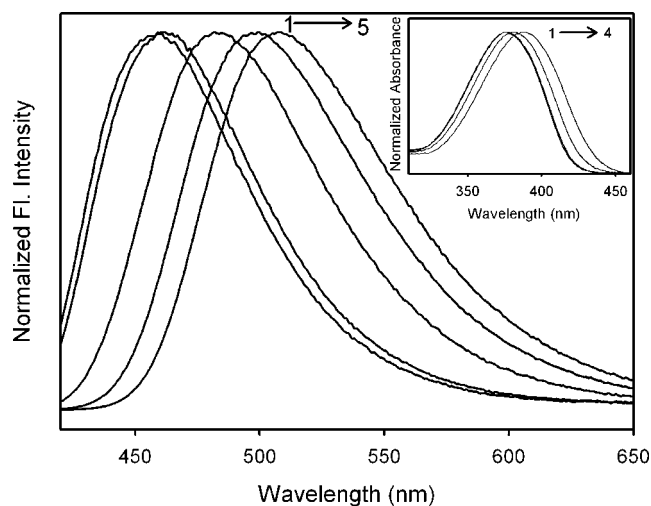


**Figure 1.** Absorption (inset) and emission spectra of C500 in water–DX mixture with different concentrations of water:  $X_W = 0.005$  (1),  $0.025$  (2),  $0.2$  (3),  $0.54$  (4), and  $0.826$  (5).

crystal ( $1\text{ mm BBO}$ ,  $\theta = 25^\circ$ ,  $\phi = 90^\circ$ ). The fluorescence emitted from the sample was upconverted in a nonlinear crystal ( $0.5\text{ mm BBO}$ ,  $\theta = 10^\circ$ ,  $\phi = 90^\circ$ ) using a gate pulse of the fundamental beam. The upconverted light is dispersed in a double monochromator and detected using photon-counting electronics. A cross-correlation function obtained by using the Raman scattering from water displayed a full width at half-maximum (fwhm) of  $165\text{ fs}$ . The femtosecond fluorescence decays were fitted using a Gaussian shape for the exciting pulse. The details of the temperature dependent picosecond-resolved spectroscopic measurement and the construction of time-resolved emission spectra (TRES) can be found elsewhere.<sup>49</sup> The time dependent fluorescence Stokes shifts, as estimated from TRES, were used to construct the normalized spectral shift correlation function or the solvent correlation function  $C(t)$ , defined as

$$C(t) = \frac{\nu(t) - \nu(\infty)}{\nu(0) - \nu(\infty)} \quad (1)$$

where  $\nu(0)$ ,  $\nu(t)$ , and  $\nu(\infty)$  are the emission maximum (in  $\text{cm}^{-1}$ ) at time zero,  $t$ , and infinity, respectively. The  $\nu(\infty)$  values have been taken to be the emission frequency beyond which an insignificant or no spectral shift is observed. The  $C(t)$  function represents the temporal response of the solvent relaxation process, as occurs around the probe following its photoexcitation and the associated change in the dipole moment. For anisotropy ( $r(t)$ ) measurements, emission polarization was adjusted to be parallel or perpendicular to that of the excitation, and anisotropy is defined as<sup>50</sup>

$$r(t) = \frac{[I_{\text{para}} - I_{\text{perp}}]}{[I_{\text{para}} + 2 \times I_{\text{perp}}]} \quad (2)$$

## Results and Discussion

Figure 1 depicts the steady-state absorption and emission spectra of C-500 in the different water–DX mixtures studied. As can be observed from the inset of the figure, the dilute samples ( $X_W = 0.005$  and  $0.025$ , where  $X_W$  is the mole fraction of water in the DX mixture) peak at  $\sim 370\text{ nm}$ , and as the water concentration in the mixture increases, a progressive red shift

of the absorption peak is produced. In the emission spectra (excited at 409 nm), a similar red shift of the peak with increasing  $X_W$  is observed. It can be argued that with increasing water content the probe experiences more polar environment which produces the observed red shift. Previously, Molotsky et al.<sup>41</sup> and Mukherjee et al.<sup>40</sup> reported a similar red shift with  $X_W$  in the emission spectra of coumarin 153 and 4-aminophthalimide (4-AP), respectively, for the water–DX mixture. It is observed that the change in emission maximum does not follow a linear relation with  $X_W$  (figure not shown). The nonlinearity might arise from the nonlinear dependence of the dielectric constant of the mixture on the mole fraction of water.<sup>40,51</sup> To understand the relative contribution of the fluorescence signal of C-500 coming from its different possible locations, we deconvolute the emission spectrum of  $X_W = 0.2$  into two curves, and the spectrum is very well fitted with two curves with peak positions at 473 and 508 nm, respectively (Figure S1, Supporting Information). The relative contributions of the curves are 47% and 53%, respectively. When deconvoluted into three curves, it produces peaks at 466 nm (33%), 495 nm (27%), and 514 nm (40%). Note that C-500 produces emission peaks at 455 and 508 nm in pure DX and water, respectively (inset of Figure S1, Supporting Information). We try to force fit the curve into two with peak positions of 455 and 508 nm. But the fitting produces very poor results (figure not shown). Also in the three-curve fitting, the peak positions do not resemble either DX or water. Thus the deconvolution study confirms that the fluorescence signal obtained is coming only from either the DX–water interface (corresponding to a peak position of 473 nm, which is in between the two bulk phases) or the water phase (corresponding to a peak position of 508 nm).

To understand the dynamics of water in the mixture, we begin with the dilute solutions ( $X_W = 0.005$  and  $0.02$ ) consisting of small clusters as evidenced from the LLS<sup>20</sup> and IR studies.<sup>42</sup> We also studied the size of the clusters using dynamic light scattering experiments and found that for dilute regions the cluster size is small ( $\sim 1$  nm, Figure S2, Supporting Information). Figure 2a depicts the femtosecond-resolved fluorescence decay transients of C500 in  $X_W = 0.005$  mixture excited at 410 nm. It is observed that the fluorescence transient at 440 nm (blue end) can be fitted with four decay components of 0.4, 2.7, 14.2, and 1500 ps. On the other hand, the transient at 550 nm is fitted with two rise components of 1.1 and 110 ps along with a long decay component of 1700 ps. The observed difference in the decay pattern of the transients at blue and red ends clearly indicates solvation of the probe. Figure 2b (inset) denotes the constructed TRES of the system. The observed Stokes shift is relatively small ( $450\text{ cm}^{-1}$ ) and eventually finishes at 20 ps. The constructed solvation correlation function,  $C(t)$ , can be fitted biexponentially with time constants of 0.3 ps (60%) and 3.7 ps (40%) (Table 1). The solvation time constants are also fast for the  $X_W = 0.025$  system with considerably small Stokes shift ( $550\text{ cm}^{-1}$ ) and time constants of 0.55 ps (50%) and 5.65 ps (50%) (Table 1). Thus in the dilute region ( $X_W = 0.005$  and  $0.025$ ), the solvation dynamics is fast with time constants of several hundreds of femtoseconds and a few picoseconds. It is evident from IR studies<sup>42</sup> that the water structure in the dilute region considerably differs from that in the concentrated region, wherein the water present in the cluster resembles that of the bulk water, whereas in the former system weakly hydrogen-bonded water molecules in the form of small clusters are present with considerably different geometry than that in the bulk water due to the breakage of the hydrogen bond network.<sup>52</sup>

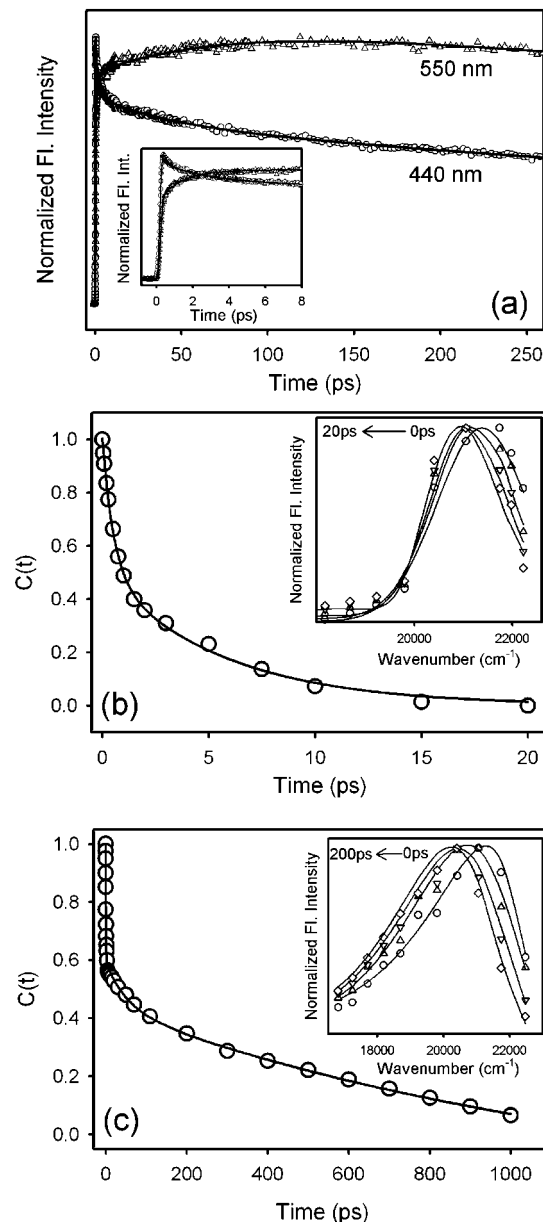


**Figure 2.** (a) Femtosecond-resolved decay transients of C500 at 440 and 550 nm in water–DX mixture with  $X_W = 0.005$ . (b) Solvent correlation function,  $C(t)$ , of C500 in water–DX mixture with  $X_W = 0.005$ . The corresponding TRES has been shown in the inset. (c) Solvent correlation function,  $C(t)$ , of C500 in water–DX mixture with  $X_W = 0.2$ . The corresponding TRES has been shown in the inset.

**TABLE 1: Femtosecond/Picosecond-Resolved Solvent Correlation Function Time Scales<sup>a</sup> for Water–Dioxane Mixtures at Different Water Concentrations**

| $X_{\text{water}}$ | $\tau_1$ (ps) | $\tau_2$ (ps) | $\tau_3$ (ps) | $a_1$ | $a_2$ | $a_3$ |
|--------------------|---------------|---------------|---------------|-------|-------|-------|
| 0.005 <sup>b</sup> | 0.30          | 3.70          | —             | 0.60  | 0.40  | —     |
| 0.025 <sup>b</sup> | 0.55          | 5.65          | —             | 0.50  | 0.50  | —     |
| 0.2 <sup>b</sup>   | 0.40          | 5.10          | 500           | 0.20  | 0.20  | 0.60  |
| 0.2 <sup>c</sup>   | 150           | 510           | —             | 0.67  | 0.33  | —     |
| 0.54 <sup>c</sup>  | 30            | 200           | —             | 0.30  | 0.70  | —     |
| 0.826 <sup>c</sup> | 20            | 135           | —             | 0.36  | 0.64  | —     |

<sup>a</sup> Error in time scale  $\pm 10\%$ . <sup>b</sup> Results obtained from femtosecond setup. <sup>c</sup> Results obtained from picosecond setup.

Let us now focus on the origin of the observed solvation components. The slower of the two components (which is of the order of a few picoseconds) may be identified with the

cooperative relaxation of the hydrogen bond network of water (relaxation time of 8.4 ps in neat water).<sup>32</sup> Molecular dynamic simulation shows that such relaxation originates from the clusters comprising of 10–40 water molecules.<sup>53,54</sup> However, the presence of DX, which can act as a hydrogen bond donor (but not an acceptor), affects the hydrogen bond network relaxation process. <sup>17</sup>O NMR studies show that the reorientational correlation time of water is considerably reduced when entrapped in an isolated form in a hydrophobic solvent (nitromethane) as the activation energy for such motion is reduced by 2.3 kJ mol<sup>-1</sup> due to the confinement.<sup>30</sup> In the present study the observed time constants of 3.7 ps (for  $X_W = 0.005$ ) and 5.65 ps (for  $X_W = 0.02$ ) corroborate with this finding. A recent dielectric relaxation study<sup>16</sup> reports a similar increase in the time scale and amplitude of this mode of relaxation with increase in water content in the dilute region of water–DX mixture. The faster subpicosecond time scale mainly arises due to the relaxation of water molecules that are not part of the tetrahedral hydrogen bond network<sup>52</sup> of the small water clusters, but reside in the DX-rich region either in the free state or by forming weak hydrogen bonds with the ether oxygen of DX,<sup>16</sup> which is fast (0.4 ps) in pure water.<sup>32</sup> Thus the observed fast component might be due to the water molecules residing on the surface of the clusters. It could be noted here that solvation dynamics in pure DX has been reported by Maroncelli et al.<sup>55</sup> using coumarin 153 probe, and it was found to be an ultrafast process with components of 0.18 and 2.2 ps, a time scale much faster than that reported for the present mixed solvent systems (Table 1). In the present study, however, it is expected that the solvation will be governed by the water molecules rather than the DX molecules since a dipolar solvent is preferred over a quadrupolar solvent in the solute–solvent interaction.<sup>37</sup>

The solvation of relatively concentrated solution ( $X_W = 0.2$ ) has been found to be slower. Figure 2c depicts the constructed TRES and  $C(t)$  of the  $X_W = 0.2$  system. As can be observed from the figure,  $C(t)$  can be fitted triexponentially with time components of 0.36 ps (30%), 5.1 ps (20%), and 490 ps (50%) (Table 1) with a Stokes shift of 1500 cm<sup>-1</sup>. To have a better understanding of the slow dynamics of the concentrated systems, we perform picosecond-resolved fluorescence spectroscopy of all the mixed systems using a TCSPC setup. It is observed that for the dilute systems ( $X_W = 0.005$  and 0.025), there is almost no change in the decay pattern of the transients in the red and blue ends (data not shown). The solvation dynamics might be too fast to be detected in our TCSPC setup. Figure 3a (inset) depicts the fluorescence transients of the  $X_W = 0.2$  system at blue and red ends. The decay transient at 430 nm (blue end) is fitted triexponentially with time constants of 100, 400, and 5100 ps. The 480 nm transient is biexponentially fitted with time constants of 340 and 5100 ps. The transient in the red end (610 nm) produces a considerable rise component of 310 ps along with a decay component of 5170 ps. The difference in transients in the red and blue ends clearly points to the presence of solvation in the system. Figure 3a depicts the constructed TRES, and the corresponding  $C(t)$  can be fitted biexponentially with time constants of 150 ps (67%) and 510 ps (33%) (Table 1) and with a Stokes shift of 750 cm<sup>-1</sup>. The average time constant ( $\langle\tau_s\rangle = a_1\tau_1 + a_2\tau_2$ ) of 270 ps is in good agreement with that reported by Molotosky et al.<sup>41</sup> with coumarin 153 for an identical system. With an increase in the water concentration, the dynamics becomes faster (Figure 3b). For the  $X_W = 0.54$  system, the correlation function is fitted biexponentially with time constants of 30 ps (30%) and 200 ps (70%) (Table 1) with a Stokes shift of 600 cm<sup>-1</sup>, whereas for the  $X_W = 0.826$  system

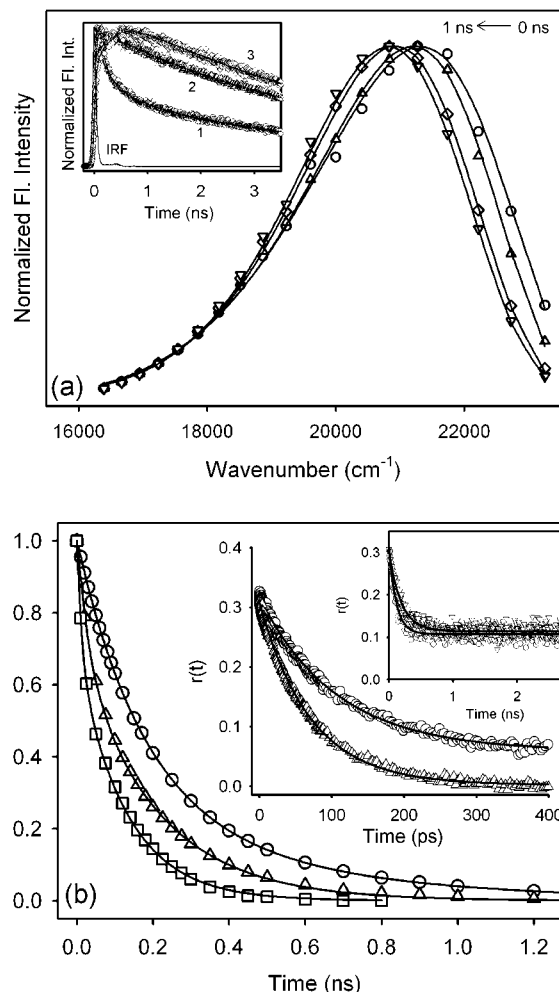


**Figure 3.** (a) TRES of C500 in water–DX mixture with  $X_W = 0.2$ . The picosecond-resolved decay transients at 430 nm (1), 480 nm (2), and 610 nm (3) are shown in the inset. (b) Solvent correlation function,  $C(t)$ , of C500 in water–DX mixture with  $X_W = 0.2$  (open circle), 0.54 (open triangle), and 0.826 (open square). (Inset) Femto- and picosecond-resolved rotational anisotropy for the  $X_W = 0.005$  (open triangle), 0.2 (open circle), and 0.54 (open down triangle) systems.

the time constants are 20 ps (36%) and 135 ps (64%) (Table 1) with a 300 cm<sup>-1</sup> Stokes shift. The faster components of these two systems corroborate well with those observed from the femtosecond studies (15.3 and 11.5 ps, respectively).

It is interesting to note that for the smaller clusters ( $X_W = 0.005$  and 0.02), the dynamics was fast, and as the cluster grows in size (for  $X_W = 0.2$ , the cluster size is of the order of 200 nm, Figure S2, Supporting Information), a slow component of hundreds of picoseconds arises, which in turn decreases with increasing water concentration. Such slow solvation dynamics in relatively concentrated solutions of a polar fluid in hydrophobic solvents has previously been reported.<sup>39–41</sup> This slow component might have its genesis in the translational diffusion of water into the solvation shell displacing the nonpolar solvent molecules in the cluster.<sup>41,56,57</sup> Also the decrease in  $\tau_{\text{slow}}$  with increasing water content is associated with the increasing average mutual diffusion coefficient ( $\langle D_m \rangle$ ) as the increase in water content in a water–DX mixture increases the number of hydrogen bonds per oxygen atom and also the relaxation rate.<sup>22</sup> It can be argued that the dynamic exchange between the less mobile bound type (strongly hydrogen-bonded) water molecules with free type (weakly hydrogen-bonded or partially bonded to the ether oxygen of DX) in the cluster produces the observed

slow dynamics. A detailed study of this exchange equilibrium and the corresponding energetics has been discussed in a later section.

We measure the rotational anisotropy of the mixtures with both picosecond- and femtosecond-resolved setup (Figure 3b, inset). For the dilute mixture ( $X_W = 0.005$ ), the observed femtosecond-resolved anisotropy can be fitted single exponentially with a time constant ( $\tau_r$ ) of 65 ps. If we assume that the probe is located at the edge of the cluster, then the microviscosity as experienced by the probe at the cluster interface can be calculated from the  $\tau_r$  data by using the well-known Debye–Stokes–Einstein equation

$$\tau_r = \frac{\eta V}{k_b T} \quad (3)$$

where  $\eta$  is the microviscosity experienced by the probe and  $V$  is molecular volume of the probe. Assuming the approximate diameter of the probe to be 0.6 nm and putting the experimentally obtained value of  $\tau_r$  in eq 3, the microviscosity is calculated to be 2.3 cP. This value is on the same order of magnitude as that obtained in encapsulated water molecules for reverse micelles.<sup>58</sup> It is to be noted that the probe is only sparingly soluble in water and remains mainly in the DX phase in the ground state. In the excited state, however, it moves to the aqueous phase and as discussed earlier (Figure S1, Supporting Information), the fluorescence signal is generated only by the probe molecules located either at the DX–water interface or in the aqueous phase, and thus it experiences a slightly larger microviscosity than the corresponding bulk phases. It is important to note that the obtained  $\eta$  value is only the microviscosity experienced by the probe molecules and might not reflect the viscosity of the total systems. The anisotropy decay for the concentrated system ( $X_W = 0.2$ ) is associated with a time constant of 110 ps along with a considerable offset value, which points out that the cluster size is large enough not to be fully rotated within the experimental time window. We perform picosecond-resolved anisotropy experiments for the concentrated systems (Figure 3b, inset) and found that for the  $X_W = 0.2$  system, the decay can be fitted with a time constant of 110 ps with an offset (34%). The G factor<sup>50</sup> used for the anisotropy measurement has been calculated from the corresponding femtosecond-resolved measurements. The calculated microviscosity at the interface for this composition is 4.0 cP, which is about twice the value of the dilute system wherein the hydrogen bond formation is perturbed, which might cause the lower microviscosity. With the increase in the number of water molecules in the cluster, hydrogen bond formation ability increases resulting in an increase in  $\tau_r$  and increased microviscosity. For a more concentrated system ( $X_W = 0.54$ ), the decay becomes slower (with time constant of 180 ps) with a considerable offset value (38%) indicating the formation of a larger cluster with higher microviscosity at the interface. The presence of considerable offset value in the picosecond-resolved rotational anisotropy decay indicates the size of the cluster to be large.

To understand the nature of hydrogen bond formation and the possible equilibrium between the two types of water present in the cluster, we measure solvation dynamics of the  $X_W = 0.2$  system at different temperature (in the temperature window of 15–70 °C) using C500 probe. Such temperature dependent solvation dynamics study has not yet been reported for the water–DX mixture. This mole fraction ( $X_W = 0.2$ ) is of interest as earlier IR studies revile sharp change in the water stretching frequencies around this composition.<sup>42</sup> The steady-state emission

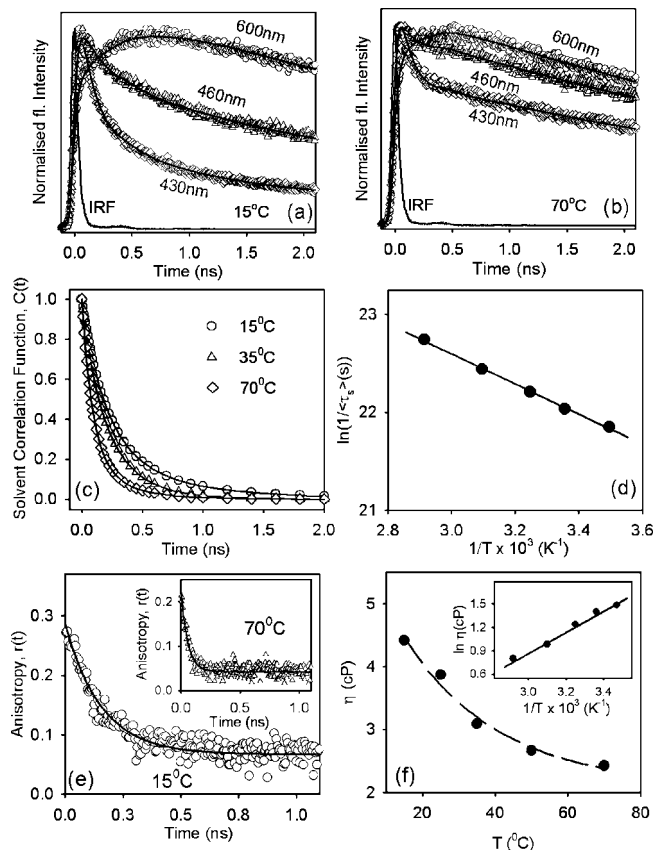


**Figure 4.** (a) Picosecond-resolved decay transients at 430, 460, and 600 nm of C500 in water–DX mixture with  $X_W = 0.2$  at 15 °C. (b) The picosecond-resolved decay transients at 430, 460, and 600 nm of C500 in water–DX mixture with  $X_W = 0.2$  at 70 °C. (c) TRES of C500 in water–DX mixture with  $X_W = 0.2$  at 15°, 35°, and 70 °C. (d) Arrhenius plot for water–DX mixture with  $X_W = 0.2$ . The solid line is the best fit straight line. (e) Picosecond-resolved rotational anisotropy for water–DX mixture with  $X_W = 0.2$  at 15 and 70 °C. (f) Microviscosity of water–DX mixture with  $X_W = 0.2$  as a function of temperature. The broken line is a guide to the eyes. An Arrhenius plot for the same has been shown in the inset. The solid line is the best fit straight line.

spectra of the system show a marginal (3–4 nm) blue shift as the temperature is increased from 15 to 70 °C (figure not shown). The observed blue shift indicates a less polar environment to be experienced by the probe at elevated temperature. A possible breakdown of the hydrogen bond network followed by the formation of smaller clusters with increasing temperature (Figure S2, Supporting Information) might have been responsible for the decreased polarity. Figure 4a, b shows the fluorescence decay transients of C500 at 15 and 70 °C, respectively. The figure depicts considerable difference between the decay patterns at particular wavelengths clearly indicating a temperature dependency on solvation behavior. We construct the TRES at different temperatures, and the corresponding  $C(t)$  values are fitted biexponentially. A representative figure is presented (Figure 4c), and the fitting parameters are given in Table 2. It is observed that solvation dynamics gets faster with increasing temperature, and the probe molecules are solvated with faster moving water molecules at higher temperature. It clearly indicates that at elevated temperature the hydrogen bond network present in the bulklike cluster breaks down and isolated small clusters consisting of weakly hydrogen-bonded water molecules start growing, producing the faster solvation dynamics.

In the previous section, we discussed the possible equilibrium in cluster wherein bound type (strongly hydrogen-bonded) water

**TABLE 2: Picosecond-Resolved Solvent Correlation Function Time Scales<sup>a</sup> for Water–Dioxane Mixtures with  $X_W = 0.2$  at Different Temperatures**

| $T$ (°C) | $\tau_1$ (ns) | $a_1$ | $\tau_2$ (ns) | $a_2$ | $\langle 120 \rangle$ (ns) |
|----------|---------------|-------|---------------|-------|----------------------------|
| 15       | 0.19          | 0.71  | 0.65          | 0.29  | 0.32                       |
| 25       | 0.15          | 0.67  | 0.51          | 0.33  | 0.27                       |
| 35       | 0.14          | 0.49  | 0.31          | 0.51  | 0.23                       |
| 50       | 0.11          | 0.30  | 0.21          | 0.70  | 0.18                       |
| 70       | 0.08          | 0.69  | 0.25          | 0.31  | 0.13                       |

<sup>a</sup> Error in time scale  $\pm 10\%$ .

molecules are in equilibrium with free type (weakly hydrogen-bonded or partially bonded to the ether oxygen of DX). The rate constant for bound-to-free interconversion ( $k_{\text{bf}}$ ) is related to the solvation time constant ( $\langle \tau_s \rangle$ ) according to the following relations<sup>40,59,60</sup>

$$k_{\text{bf}} \approx \frac{1}{\langle \tau_s \rangle} = \left( \frac{k_{\text{b}} T}{h} \right) \exp\left( \frac{-\Delta G}{RT} \right) \quad (4)$$

where  $\Delta G$  is the activation energy for solvation dynamics in the mixture. Assuming that the bound-to-free water equilibrium follows an Arrhenius type of barrier crossing model, we plot  $\ln(1/\langle \tau_s \rangle)$  as a function of  $1/T$ , and a good linear fit is obtained (Figure 4d). From the slope of the straight line, the activation energy ( $E_{\text{act}}$ ) is calculated to be  $3.1 \pm 0.3$  kcal mol<sup>-1</sup>. Previously, Mukherjee et al.<sup>40</sup> reported an activation energy of 4.7 kcal mol<sup>-1</sup> for water–DX mixture at  $X_W = 0.22$ . This value is on the order of hydrogen bond energy in bulk water ( $\sim 5$  kcal mol<sup>-1</sup>)<sup>61,62</sup> and is in turn slightly higher than the value obtained in the present study. The observed  $E_{\text{act}}$  value is smaller than the bulk hydrogen bond energy and therefore must be associated with some other bonding pattern. It should be remembered that the probe used by Mukherjee et al.<sup>40</sup> (4-AP) is different from that used by us. 4-AP is highly soluble in water and preferentially resides within the core of the water clusters, and photoexcitation of it provides information on bulk water only. On the other hand, C500 provides information on the cluster interface. DX molecules in their chair conformation bind with water molecules with H(water).....O(ether oxygen of DX) bond energy of  $\sim 2.3$  kcal mol<sup>-1</sup>,<sup>63</sup> which is in turn less than the  $E_{\text{act}}$  value obtained in the present study. As C500 is primarily located at the cluster edge and moves toward the core of the cluster upon excitation, it provides integrated information on DX–water hydrogen bond at the interface and water–water tetrahedral bond in the bulk. Thus, the observed  $E_{\text{act}}$  value of 3.1 kcal mol<sup>-1</sup> is in between the two expected values of 2.3 and 5.0 kcal mol<sup>-1</sup>.

To obtain a better understanding of the microenvironment of the clusters, we measure the rotational anisotropy of the same system at different temperatures. A representative figure is depicted (Figure 4e) for 15 and 70 °C. As observed from the figure,  $\tau_r$  becomes faster upon increasing the temperature. We measure the microviscosity ( $\eta$ ) at different temperatures using eq 3, and  $\eta$  is plotted as a function of temperature (Figure 4f). It is observed that  $\eta$  decreases gradually with increasing temperature revealing that the probe experiences less rotational hindrance at higher temperature. The breaking of water–water hydrogen bond might be the reason behind this. Assuming that microviscosity changes with temperature following the relation

$$\eta = \eta_0 \exp\left( \frac{E_\eta}{RT} \right) \quad (5)$$

where  $E_\eta$  is the energy barrier for the viscous flow, we plot  $\ln \eta$  against  $1/T$  (inset of Figure 4f), and a good linear fit is obtained with a calculated  $E_\eta$  value of  $2.6 \pm 0.3$  kcal mol<sup>-1</sup>. Note that this  $E_\eta$  value is smaller than that of bulk water (3.9 kcal mol<sup>-1</sup>). This difference in  $E_\eta$  values confirms our previous conclusion that at the cluster interface there exists heterogeneous hydrogen bonding between the ether oxygen of DX and water along with water–water hydrogen bond, and breaking–remaking of such bonds contributes to the slow solvation in concentrated water–DX mixture.

## Conclusions

Our studies follow the modification of solvation dynamics of water molecules in nonpolar DX with the structural changes in the clusters and temperature. The fast solvation dynamics observed in the small clusters (for low water concentration systems) is due to the various modes of rotational relaxation of water molecules present in the isolated small water clusters. On the other hand, the slow dynamics of the concentrated solutions is due to the translational diffusion of water molecules along the large clusters. Solvation dynamics becomes faster with increasing temperature for the concentrated system due to the breakage of tetrahedral hydrogen bond network in the clusters. The activation energy for the process has been calculated to be 3.1 kcal mol<sup>-1</sup>, which is smaller than the hydrogen bond energy in bulk water but larger than the water–DX hydrogen bond energy, confirming the presence of both kinds of bond at the cluster interface.

**Acknowledgment.** We thank DST for financial grant (SR/FTP/PS-05/2004, SR/SO/BB-15/2007). P.K.V. thanks CSIR for providing a research fellowship.

**Supporting Information Available:** Figures S1 and S2. This material is available free of charge via the Internet at <http://pubs.acs.org>.

## References and Notes

- (1) Jeffrey, G. A. *An Introduction to Hydrogen Bonding*; Oxford University Press: New York, 1997.
- (2) Franks, F. *Water: A Comprehensive Treatise*; Plenum: New York, 1972.
- (3) Stillinger, F. H. *Science* **1980**, *209*, 451–457.
- (4) Nibbering, E. T. J.; Elsaesser, T. *Chem. Rev.* **2004**, *104*, 1887–1914.
- (5) Cowan, M. L.; Bruner, B. D.; Huse, N.; Dwyer, J. R.; Chugh, B.; Nibbering, E. T. J.; Elsaesser, T.; Miller, R. J. D. *Nature* **2005**, *434*, 199–202.
- (6) Ashihara, S.; Huse, N.; Espagne, A.; Nibbering, E. T. J.; Elsaesser, T. *J. Phys. Chem. A* **2007**, *111*, 743–746.
- (7) Kraemer, D.; Cowan, M. L.; Paarmann, A.; Huse, N.; Nibbering, E. T. J.; Elsaesser, T.; Miller, R. J. D. **2008**, *105*, 437–442.
- (8) Cringus, D.; Jansen, T. C.; Pshenichnikov, M. S.; Wiersma, D. A. *J. Chem. Phys.* **2007**, *127*, 084507.
- (9) Cringus, D.; Yermenko, S.; Pshenichnikov, M. S.; Wiersma, D. A. *J. Phys. Chem. B* **2004**, *108*, 10376–10387.
- (10) Lindner, J.; Cringus, D.; Pshenichnikov, M. S.; Voehringer, P. *Chem. Phys.* **2007**, *341*, 326–335.
- (11) Asbury, J. B.; Steinel, T.; Stromberg, C.; Corcelli, S. A.; Lawrence, C. P.; Skinner, J. L.; Fayer, M. D. *J. Phys. Chem. A* **2004**, *108*, 1107–1119.
- (12) Fecko, C. J.; Eaves, J. D.; Loparo, J. J.; Tokmakoff, A.; Geissler, P. L. *Science* **2003**, *301*, 1698–1702.
- (13) Woutersen, S.; Bakker, H. J. *Nature* **1999**, *402*, 507–509.
- (14) Kropman, M. F.; Bakker, H. J. *Science* **2001**, *291*, 2118–2120.
- (15) Asbury, J. B.; Steinel, T.; Kwak, K.; Corcelli, S. A.; Lawrence, C. P.; Skinner, J. L.; Fayer, M. D. *J. Chem. Phys.* **2004**, *121*, 12431–12446.
- (16) Schrodle, S.; Fischer, B.; Helm, H.; Buchner, R. *J. Phys. Chem. A* **2007**, *111*, 2043–2046.
- (17) Schrodle, S.; Hefter, G.; Buchner, R. *J. Phys. Chem. B* **2007**, *111*, 5946–5955.

- (18) Keutsch, F. N.; Saykally, R. J. *Proc. Natl. Acad. Sci. U.S.A.* **2001**, *98*, 10533–10540.
- (19) Mashimo, S.; Miura, N.; Umehara, T.; Yagihara, S.; Higasi, K. *J. Chem. Phys.* **1992**, *96*, 6358–6361.
- (20) Yang, C.; Li, W.; Wu, C. *J. Phys. Chem. B* **2004**, *108*, 11866–11870.
- (21) Takamuku, T.; Yamaguchi, A.; Tabata, M.; Nishi, N.; Yoshida, K.; Wakita, H.; Yamaguchi, T. *J. Mol. Liq.* **1999**, *83*, 163–177.
- (22) Takamuku, T.; Nakamizo, A.; Tabata, M.; Yoshida, K.; Yamaguchi, T.; Otomo, T. *J. Mol. Liq.* **2003**, *103*, 143–159.
- (23) Vaitheeswaran, S.; Yin, H. C.; Rasiaiah, J. C.; Hummer, G. *Proc. Natl. Acad. Sci. U.S.A.* **2004**, *101*, 17002–17005.
- (24) Toxvaerd, S. *J. Chem. Phys.* **1981**, *74*, 1998–2005.
- (25) Schoen, M.; Cushman, J. H.; Diestler, D. J.; Rhykerd, C. L., Jr. *J. Chem. Phys.* **1988**, *88*, 1394–1406.
- (26) Murad, S.; Ravi, P.; Powles, J. G. *J. Chem. Phys.* **1993**, *98*, 9771–9781.
- (27) Liu, K.; Cruzan, J. D.; Saykally, R. J. *Science* **1996**, *271*, 929–933.
- (28) Gruenloh, C. J.; Carney, J. R.; Arrington, C. A.; Zwier, T. S.; Fredericks, S. Y.; Jordan, K. D. *Science* **1997**, *276*, 1678–1681.
- (29) Nauta, K.; Miller, R. E. *Science* **2000**, *287*, 293–295.
- (30) Price, W. S.; Ide, H.; Arata, Y. *J. Chem. Phys.* **2000**, *113*, 3686.
- (31) Hummer, G.; Rasiaiah, J. C.; Noworyta, J. P. *Nature* **2001**, *414*, 188–190.
- (32) Fukasawa, T.; Sato, T.; Watanabe, J.; Hama, Y.; Kunz, W.; Buchner, R. *Phys. Rev. Lett.* **2005**, *95*, 197802.
- (33) Starr, F. W.; Nielsen, J. K.; Stanley, H. E. *Phys. Rev. Lett.* **1999**, *82*, 2294–2297.
- (34) Starr, F. W.; Nielsen, J. K.; Stanley, H. E. *Phys. Rev. E* **2000**, *62*, 579–587.
- (35) Gardecki, J. A.; Maroncelli, M. *Chem. Phys. Lett.* **1999**, *301*, 571–578.
- (36) Jarzeba, P. W.; Walker, G. C.; Johnson, A. E.; Barbara, P. F. *Chem. Phys.* **1991**, *152*, 57–68.
- (37) Luther, B. M.; Kimmel, J. R.; Levinger, N. E. *J. Chem. Phys.* **2002**, *116*, 3370–3377.
- (38) Ladanyi, B. M.; Perng, B. C. *J. Phys. Chem. A* **2002**, *106*, 6922–6934.
- (39) Sahu, K.; Mondal, S. K.; Roy, D.; Karmakar, R.; Bhattacharyya, K. *J. Photochem. Photobiol., A* **2005**, *172*, 180–184.
- (40) Mukherjee, S.; Sahu, K.; Roy, D.; Mondal, S. K.; Bhattacharyya, K. *Chem. Phys. Lett.* **2004**, *384*, 128–133.
- (41) Molotsky, T.; Huppert, D. *J. Phys. Chem. A* **2003**, *107*, 8449–8457.
- (42) Sirotkin, V. A.; Solomonov, B. N.; Faizullin, D. A.; Fedotov, V. D. *J. Struct. Chem.* **2000**, *41*, 997–1003.
- (43) Pimentel, G. C.; McClellan. *The Hydrogen Bond*; Freeman: San Francisco, CA, 1960.
- (44) Majumder, P.; Sarkar, R.; Shaw, A. K.; Chakraborty, A.; Pal, S. K. *J. Colloid Interface Sci.* **2005**, *290*, 462–474.
- (45) Mitra, R. K.; Sinha, S. S.; Pal, S. K. *Langmuir* **2008**, *24*, 49–56.
- (46) Narayanan, S. S.; Sinha, S. S.; Sarkar, R.; Pal, S. K. *J. Phys. Chem. B* **2008**, *112*, 2859–2867.
- (47) Narayanan, S. S.; Sinha, S. S. R.; Sarkar, R.; Pal, S. K. *Chem. Phys. Lett.* **2008**, *452*, 99–104.
- (48) Mitra, R. K.; Sinha, S. S.; Verma, P. K.; Pal, S. K. *J. Phys. Chem. B* **2008**, *112*, 12946–12953.
- (49) Mitra, R. K.; Sinha, S. S.; Pal, S. K. *J. Phys. Chem. B* **2007**, *111*, 7577–7581.
- (50) Lakowicz, J. R. *Principles of Fluorescence Spectroscopy*; Kluwer Academic/Plenum: New York, 1999.
- (51) Suppan, P. *J. Chem. Soc., Faraday Trans. 1* **1987**, *83*, 495–510.
- (52) Ramachandran, C. N.; Sathyamurthy, N. *Chem. Phys. Lett.* **2005**, *410*, 348–351.
- (53) Tanaka, H.; Ohmine, I. *J. Chem. Phys.* **1987**, *87*, 6128–6139.
- (54) Ohmine, I.; Tanaka, H.; Wolynes, P. G. *J. Chem. Phys.* **1988**, *89*, 5852–5860.
- (55) Horng, M. L.; Gardecki, J. A.; Papazyan, A.; Maroncelli, M. *J. Phys. Chem.* **1995**, *99*, 17311–17337.
- (56) Cichos, F.; Willert, A.; Rempel, U.; von Borczyskowski, C. *J. Phys. Chem. A* **1997**, *101*, 8179–8185.
- (57) Chandra, A.; Bagchi, B. *J. Chem. Phys.* **1991**, *94*, 8367–8377.
- (58) Corbeil, E. M.; Riter, R. E.; Levinger, N. E. *J. Phys. Chem. B* **2004**, *108*, 10777–10784.
- (59) Nandi, N.; Bhattacharyya, K.; Bagchi, B. *Chem. Rev.* **2000**, *100*, 2013–2045.
- (60) Nandi, N.; Bagchi, B. *J. Phys. Chem. B* **1997**, *101*, 10954–10961.
- (61) Moore Plummer, P. L. *J. Mol. Struct. THEOCHEM* **1997**, *417*, 35–47.
- (62) Feyereisen, M. W.; Feller, D.; Dixon, D. A. *J. Phys. Chem.* **1996**, *100*, 2993–2997.
- (63) Buz'ko, V. Y.; Sukhno, I. V.; Panyushkin, V. T.; Ramazanova, D. N. *J. Struct. Chem.* **2005**, *46*, 596–602.